NEOPLASIA
www.neoplasia.com

Volume 28 Number xxx Month 2022 pp. 100790

Phenotypic and molecular states of IDH1 mutation-induced CD24-positive glioma stem-like cells

Sara Haddock[a,b]; Tyler J. Alban[c]; Şevin Turcan[d]; Hana Husic[c]; Eric Rosiek[e]; Xiaoxiao Ma[c]; Yuxiang Wang[f]; Tejus Bale[g]; Alexis Desrichard[b]; Vladimir Makarov[c]; Sebastien Monette[h]; Wei Wu[b]; Rui Gardner[i]; Katia Manova[e]; Adrienne Boire[b]; Timothy A. Chan[b,c,j,*]

[a] Weill Cornell School of Medicine, New York, NY 10021, USA
[b] Human Oncology and Pathogenesis Program, Memorial Sloan Kettering Cancer Center, New York, NY 10065, USA
[c] Center for Immunotherapy and Precision Immuno-Oncology, Cleveland Clinic, Cleveland, OH 44022, USA
[d] Neurology Clinic and National Center for Tumor Diseases, Heidelberg University Hospital, Heidelberg, Germany
[e] Department of Molecular Cytology, Memorial Sloan Kettering Cancer Center, New York, NY 10065, USA
[f] Department of Pathology, School of Basic Medical Sciences, Fudan University, Shanghai, 200032, China
[g] Department of Pathology, Memorial Sloan Kettering Cancer Center, New York, NY 10065, USA
[h] Laboratory of Comparative Pathology, Memorial Sloan Kettering Cancer Center, The Rockefeller University, Weill Cornell Medicine, New York, NY 10065, USA
[i] Flow Cytometry Core, Memorial Sloan Kettering Cancer Center, New York, NY 10065, USA
[j] Case Western School of Medicine, Cleveland, OH 44106, USA

Abstract

Mutations in *IDH1* and *IDH2* drive the development of gliomas. These genetic alterations promote tumor cell renewal, disrupt differentiation states, and induce stem-like properties. Understanding how this phenotypic reprogramming occurs remains an area of high interest in glioma research. Previously, we showed that IDH mutation results in the development of a CD24-positive cell population in gliomas. Here, we demonstrate that this CD24-positive population possesses striking stem-like properties at the molecular and phenotypic levels. We found that CD24 expression is associated with stem-like features in IDH-mutant tumors, a patient-derived gliomasphere model, and a neural stem cell model of IDH1-mutant glioma. In orthotopic models, CD24-positive cells display enhanced tumor initiating potency compared to CD24-negative cells. Furthermore, CD24 knockdown results in changes in cell viability, proliferation rate, and gene expression that closely resemble a CD24-negative phenotype. Our data demonstrate that induction of a CD24-positive population is one mechanism by which IDH-mutant tumors acquire stem-like properties. These findings have significant implications for our understanding of the molecular underpinnings of IDH-mutant gliomas.

Neoplasia (2022) 28, 100790

Keywords: IDH1 mutation, Low-grade glioma, CD24, cancer stem cells, Neural stem cells, Orthotopic mouse model

Abbreviations: bFGF, Basic fibroblast growth factor; dox, Doxycycline; EdU, 5-Ethynyl-2′-deoxyuridine; EGF, Epidermal growth factor; FDR, False discovery rate; GBM, Glioblastoma; GSEA, Gene set enrichment analysis; hNSC, Human neural stem cell; IDH1, Isocitrate dehydrogenase 1; LGG, Low-grade glioma; MSigDB, Molecular Signatures Database; MSKCC, Memorial Sloan-Kettering Cancer Center; NCBI, National Center for Biotechnology Information; NES, Normalized enrichment score; NSG, NOD-*scid* IL2Rγ^{null}; NTC, Nontargeting control; OE, Overexpression; qRT-PCR, Quantitative real-time polymerase chain reaction; RNAseq, RNA sequencing; SEM, Standard error of the mean; TCGA, The Cancer Genome Atlas; TERT, Telomerase reverse transcriptase; WHO, World Health Organization.

* Corresponding author.
E-mail address: chant2@ccf.org (T.A. Chan).

Received 30 January 2022; received in revised form 19 March 2022; accepted 21 March 2022

https://doi.org/10.1016/j.neo.2022.100790

Introduction

Gliomas are devastating cancers that are generally considered incurable due to their extensive heterogeneity and invasive nature. Surgery, chemotherapy, and radiotherapy are the mainstays of therapy but these treatments can only provide a modest survival benefit [1,2]. Although lower-grade gliomas (LGGs) (World Health Organization [WHO] Grades II and III) are less aggressive compared to glioblastomas (GBM; WHO Grade IV), most patients experience recurrence and treatment options are eventually exhausted [3–6].

The majority of LGGs and secondary GBMs harbor a heterozygous missense mutation in isocitrate dehydrogenase 1 (*IDH1*) which changes the arginine at codon 132, most commonly to a histidine (R132H) [7–9]. Mutations of the corresponding location on *IDH2* are also present in cancers that commonly harbor IDH mutations, such as acute myeloid leukemia, but are less prevalent in gliomas [10]. Mutant IDH1 or IDH2 protein catalyzes the production of the oncometabolite 2-hydroxyglutarate [11], which induces tumor development, hypermethylation of CpG islands, and altered histone methylation [12–14]. The global epigenomic repatterning and resulting gene expression changes that typify IDH-mutant cancers result in a differentiation block and persistent upregulation of stem cell-associated pathways [12,13,15–19].

Multiple studies in cell line models of IDH mutant glioma have demonstrated that the $IDH1^{R132H}$ mutation induces *CD24* upregulation [20,21]. CD24 is expressed during early development of the central nervous system, but is absent in mature, healthy brain [22]. In the setting of cancer, CD24 has been reported as a pro-invasive factor [23,24]. Its expression is associated with shorter survival and predicts a more aggressive disease course [25,26].

Cancer stem cells are a subset of malignant cells within tumors that exhibit stem-like features, including self-renewal, multipotency, and tumor initiation potential [27,28]. Resistance to chemotherapy and radiation are common qualities associated with cancer stem cells [29–31], suggesting that stem-like tumor subpopulations may help promote recurrence and progression after treatment. CD24 is of particular interest as a marker of stemness in certain cancers. $CD24^+CD44^+$ populations in pancreatic cancers and $CD24^+CD133^+$ populations in colorectal cancers are enriched for cancer stem cells [32,33], and CD24 is sufficient to mark stem-like cells in hepatocellular and nasopharyngeal carcinomas [34–36]. Studies in neuroblastoma have found an inverse correlation between CD24 expression and degree of differentiation [22,37].

By interrogating the role of CD24 in the IDH1 mutant setting, we provide evidence that this glycoprotein marks an important glioma stem-like cell population that plays a major role in gliomas.

Materials and methods

Cell lines and culture conditions

The patient-derived gliomasphere line TS603, a gift from Cameron Brennan, is a WHO Grade III anaplastic oligodendroglioma line with 1p/19q co-deletion, an R132H mutation in endogenous *IDH1* [38,39], and a C250T *TERT* promoter mutation [40]. Tumor was obtained in accordance with institutional review board policies at Memorial Sloan-Kettering Cancer Center (MSKCC), IRB #06-107. TS603 was maintained as floating spheres in NeuroCult NS-A Proliferation medium (StemCell Technologies) supplemented with 10 ng/ml EGF, 20 ng/ml bFGF, and 2 μg/ml heparin (StemCell Technologies). Human neural stem cells (hNSCs) were grown adherently on a fibronectin coating (Sigma-Aldrich) in StemPro NSC medium (Thermo Fisher), containing Knockout DMEM/F12, StemPro Neural Supplement, 2 mM GlutaMAX-I, 20 ng/ml EGF, and 20 ng/ml bFGF. TS603s and hNSCs were passaged using Accutase, according to the manufacturer's protocol (Innovative Cell Technologies, Inc). The TS603 cell line was maintained below passage 10 for all experiments. All cell lines were routinely tested and confirmed negative for mycoplasma.

Flow cytometry and FACS

Cells in single-cell suspension were stained for 20 min with anti-human CD24 antibody (BD Biosciences; clone ML5, 555428 or 564521, 1:20). Cells were sorted using a FACSAria III, or flow cytometry was performed on an LSRFortessa or LSRII analyzer (BD Biosciences). Voltages and gates were set using appropriate fluorescence-minus-one controls. Doublet exclusion was performed with standard forward scatter/side scatter gating methods, and dead cells were excluded by DAPI staining or LIVE/DEAD Fixable Viability dye (Thermo). The anti-CD24 monoclonal antibodies used throughout this study (clones ML5 and SWA11) have been validated as specific to the protein core of CD24 [41,42].

EdU proliferation assay

An EdU proliferation kit (Abcam, ab222421) was used according to the manufacturer's instructions, with the following changes: 4% paraformaldehyde and 0.7% Tween-20 were used for fixation and permeabilization, respectively. After labeling with 10 µM EdU for 4 hours, cells were stained with anti-CD24 antibody and data was collected by flow cytometry.

TCGA RNAseq data

Hg38-aligned counts from 410 cases of *IDH1* or *IDH2* mutant and 94 IDH wild-type LGGs were downloaded from the Genomic Data Commons portal. Tumors were stratified by *CD24* expression level, with the top and bottom quartiles designated $CD24^{high}$ and $CD24^{low}$, respectively. DESeq2 was used to generate a normalized count matrix and for differential gene expression analysis. Log_2 fold change shrinkage was implemented to address variable low-level gene expression. Hierarchical clustering was performed on the top 50 upregulated and downregulated genes (greatest log_2 fold change, $p < 10e^{-10}$) using the pheatmap R package. The clusterProfiler, ReactomePA and enrichplot R packages were used for analysis and visualization of pathway enrichment with the Hallmark, KEGG, Gene Ontology and Reactome collections from MSigDB [43–45].

RNAseq and data analysis

RNA for transcriptome sequencing was isolated with Trizol-LS or RNeasy Plus Micro kit (QIAGEN). PolyA-enriched library construction and RNAseq were performed at the Integrated Genomics Operation core facility at MSKCC. Samples were run on an Illumina HiSeq 4000 or NovaSeq with 100 bp paired-end reads and a sequencing depth of about 60-80M reads per sample. Reads were aligned to hg38 using STAR [46,47]. The featureCounts read summarization program [48] was used to count mapped reads for each gene in the hg38 annotation file (gencode.v38.annotation.gtf). Count files were then merged by an in-house R script and normalized using DESeq2 [49]. DESeq2's standard differential gene expression analysis was used to compare two groups at a time ($CD24^+$ versus $CD24^-$, $CD24^+$ versus unsorted, and $CD24^-$ versus unsorted) for GSEA. For hierarchical clustering, a Likelihood Ratio Test was run in DESeq2, and clustering was performed using the pheatmap R package on the top 200 most significant (lowest adjusted p value) differentially expressed genes.

Gene set enrichment analysis

Enrichment of up- or downregulated sets of genes was computed by running GSEAPreranked [50,51] against the gene lists generated

by differential expression analysis of RNA-seq data, ranked by $\log_2$ fold-change (**Table S2**). Gene sets with between 15 and 500 members in the following MSigDB collections were used: hallmark (h.all.v5.0.symbols.gmt), C2 curated gene sets (c2.all.v5.0.symbols.gmt), C5 ontology gene sets (c5.all.v5.0.symbols.gmt), C6 oncogenic signatures (c6.all.v4.0.symbols.gmt), and C8 cell type signatures (c8.all.v7.4.symbols.gmt) [52,53]. Gene sets with NES greater than +/- 1.5 were manually assigned to categories (full gene set lists and categories can be found in **Table S1**). Leading edge analysis was run for selected gene sets to generate lists of genes that primarily contribute to that gene set's enrichment score.

In vitro *differentiation*

Cells were plated at a density of 6500 cells/cm^2 onto a coating of Growth-Factor Reduced Matrigel (Corning, 356231, diluted to approximately 300 µg/mL in PBS, incubated 2 hours at room temperature) in proliferation medium or Neurocult differentiation medium (StemCell Technologies, 05752). For cells harboring inducible shCD24 or shNTC, medium was supplemented with 100 ng/mL doxycycline hyclate. Media was changed every other day, and cells were collected and RNA extracted on day 12. Aliquots of cells from each group were reserved at the time of plating on day 0, and RNA extracted to serve as a baseline control.

qRT-PCR

RNA was purified using the RNeasy Plus kit (Qiagen) and cDNA was synthesized with the EcoDry premix (Takara Bio USA). qRT-PCR was performed in triplicate using FastStart Universal SYBR Green Master kit (Roche) on a QuantStudio 6 Flex Real-Time PCR System (Applied Biosystems). *GAPDH* was used as a normalization control. Primer pairs were designed using Primer-BLAST (NCBI). Sequences are below:

Primer Name	Sequence
GAPDH Forward	ACAACTTTGGTATCGTGGAAGG
GAPDH Reverse	GCCATCACGCCACAGTTTC
CD24 Forward	GCTCCTACCCACGCAGATTT
CD24 Reverse	GAGACCACGAAGAGACTGGC
NES Forward	GCGGGCTACTGAAAAGTTCC
NES Reverse	GAGGGTCCTGTACGTGGC
SOX2 Forward	TACAGCATGTCCTACTCGCAG
SOX2 Reverse	GAGGAAGAGGTAACCACAGGG
GFAP Forward	CTGCGGCTCGATCAACTCA
GFAP Reverse	TCCAGCGACTCAATCTTCCTC
AQP4 Forward	GGTAAGTGTGGACCTTTGTGT
AQP4 Reverse	CAAAGCAAAGGGAGATGAGAAC
S100B Forward	ACCCGCAGCAGAGACGAC
S100B Reverse	CAGCTCAGACATCCTCTTCCTT
OLIG1 Forward	CGTTAAAGTGACCAGAGCGGA
OLIG1 Reverse	CTAAAGCCGCTGGAACCGA
OLIG2 Forward	GCCCCTAAAGGTGCGGAT
OLIG2 Reverse	GGACCCGAAAATCTGGATGC
NEUROD1 Forward	GAGGCCCCAGGGTTATGAGA
NEUROD1 Reverse	TGGTCATGTTTCGATTTCCTTTGT
MAP2 Forward	CGAAGCGCCAATGGATTCC
MAP2 Reverse	TGAACTATCCTTGCAGACACCT
pac Forward	ATCGGCAAGGTGTGGGTC
pac Reverse	CTTCCATCTGTTGCTGCGC

CD24 overexpression and inducible shRNA-mediated knockdown

Human *CD24* cDNA (CCDS75499.1) was cloned into pLVX-puro (Takara). shRNA oligonucleotides targeting *CD24* or nontargeting control oligonucleotides were cloned into Tet-pLKO-puro (a gift from Dmitri Wiederschain, Addgene plasmid #21915) [54] according to the published protocol (Addgene). Lenti-X 293T cells (Takara) were transfected using FuGENE 6 reagent (Promega) with pMD2.G and psPAX2 packaging plasmids (gifts from Didier Trono, Addgene #12259 and #12260, respectively), and pLVX-puro-CD24, empty pLVX-puro vector, Tet-pLKO-puro-shCD24 or Tet-pLKO-puro-shNTC. Lentiviral particles were purified from filtered supernatant using Lenti-X Concentrator (Takara), and the viral pellet was resuspended in fresh Neurocult medium for two 12-hr transductions on consecutive days. Transduced cells were selected with puromycin. Dox dosage was titrated, and the optimal dose of 100 ng/mL was used. shRNA sequences:

Name	Target sequence (sense)
shNTC	CAACAAGATGAAGAGCACCAA
shCD24_3	GCAGTCAACAGCCAGTCTCTT
shCD24_5	CTTCTGCATCTCTACTCTTAA

Intracranial tumor implantation

Cell lines for use *in vivo* were transduced with pHIV-Luc-ZsGreen (a gift from Bryan Welm, Addgene plasmid #39196). Labeled cells were sorted for ZsGreen expression. Cells were implanted into the brains of 6-to-8-week-old female NOD-*scid* IL2Rγ^{null} mice (Jackson Laboratory), using a fixed stereotactic apparatus (Stoelting). A 1-mm burr hole was drilled into the skull using a microdrill (Harvard Apparatus) at 1.5 mm lateral and 1 mm caudal to bregma, and injections were made at a depth of 2 mm. Mice receiving injections of cells harboring inducible shCD24 or shNTC were fed dox-containing chow (doxycycline hyclate diet formulated at 625 mg/kg; Envigo) to induce expression of the hairpin.

All mouse experiments were approved by the Institutional Animal Care and Use Committee at MSKCC. Tumor-bearing mice were monitored for symptoms such as hunching, deteriorating body condition, hydrocephaly, lethargy, and neurological symptoms such as head tilt, rolling, and seizures. Symptomatic animals were sacrificed, and tissues were obtained at this time. Animals that died of unrelated causes were excluded from the study. Pathologists aided in the examination and scoring of slides: Dr. Sebastien Monette (general assessment), Dr. Tejus Bale (tumor scoring).

Bioluminescence imaging

Growth of pHIV-luc-ZsGreen-labeled xenograft tumors was monitored twice weekly by bioluminescence imaging at the MSKCC Small Animal Imaging Core. D-luciferin was injected intraperitoneally, and signal was measured using the IVIS Spectrum in vivo imaging system (PerkinElmer). Living Image software (PerkinElmer) was used for data acquisition and analysis.

Tissue Staining, slide scans

Xenograft tumor-bearing mouse brains fixed in 4% paraformaldehyde were embedded in paraffin blocks. Fluorescent immunohistochemistry of FFPE tissue sections was performed using a BOND RX automated stainer (Leica Biosystems). Detailed protocol is previously published [55]. Sections were pre-treated with Leica Bond ER2 Buffer (Leica Biosystems) for 20 min at 100C before each stain. Primary antibodies were incubated for 1 hr.

Primary antibodies were as follows: anti-CD24, clone SWA11 (a gift from Peter Altevogt, German Cancer Research Center, Heidelberg, Germany); anti-IDH1 R132H, clone H09 (Scytek); anti-CD31, clone EPR17259 (Abcam); anti-Ki-67, clone D2H10 (Cell Signaling Technology); anti-Iba1,

clone EPR16589 (Abcam); anti-PD-L1, clone E1L3N (Cell Signaling); anti-Nestin, clone 10C2 (Millipore); polyclonal anti-Olig2 (Millipore, AB9610); polyclonal anti-Sox2 (Millipore, AB5603); and polyclonal anti-S100beta (Abcam, ab41548).

Secondary antibodies were as follows: for rabbit primaries, goat anti-rabbit HRP included in the Leica Bond Refine kit (Leica, DS9800); for mouse primaries, rabbit anti-mouse IgG (Abcam), followed by goat anti-rabbit HRP from Leica Bond Refine kit. Tyramide signal amplification was performed for 10 min on Protocol F, using the following fluorescent tyramide conjugates: AF488, AF647 (Thermo, B40953 and B40958, respectively), CF543 or CF594 (Biotium, 92172 and 92174, respectively). Images were acquired using a Pannoramic 250 Flash Scanner with a 20x (NA 0.8) objective, and processed using CaseViewer software (3DHistech).

Quantitation of immunofluorescent staining

Fluorescence signal from staining of xenograft tumors was quantified using an ImageJ/Fiji [56] script designed to distinguish human tumor cells from mouse stromal cells within tumors. The script calls pixels as tumor or non-tumor based on presence or absence of the pan-tumor marker IDH1-R132H above an optimized threshold intensity, computes the total pixel area of the tumor and non-tumor, and the result is expressed as positive pixels over area. Sample masking images are shown in **Supplementary Fig. S3D**.

Generation of human neural stem cell model

pLNCX2-neo-IDH1 R132H [13] and pBabe-puro-hTERT (a gift from Bob Weinberg, Addgene plasmid #1771) were used to construct an IDH1-mutant cell model in hTERT-immortalized hNSCs [57]. 293T cells were transfected using FuGENE HD reagent (Promega) with pCL-Ampho packaging vector (Novus Biologicals, NBP2-29541) and pBabe-puro-hTERT or pLNCX2-neo-IDH1 R132H. Retroviral particles were purified from filtered supernatant using Retro-X Concentrator (Takara), the viral pellet was resuspended in fresh StemPro hNSC medium, and polybrene was added at a final concentration of 4 µg/mL. GIBCO hNSCs (Thermo, N7800-200) were sequentially transduced with the two constructs: first, wild-type hNSCs were infected with pBABE-puro-hTERT (two 4-hr incubations with retrovirus on consecutive days). One passage later, the hTERT cells were infected with pLNCX2-neo-IDH1-R132H. Doubly transduced cells were selected with puromycin and G418, and pooled populations of resistant cells expressing hTERT with IDH1 R132H were confirmed by Western blot with anti-hTERT antibody (clone Y182, Abcam) and anti-IDH1 R132H antibody (clone H09, Scytek). Expression of hTERT and mutant IDH1 was maintained in these cells for at least 50 passages (**Supplementary Fig. S2A**).

Results

CD24 is associated with a stem-like gene expression profile in the IDH1-mutant setting

We examined the expression of CD24 in glioma tumors. Among LGGs in The Cancer Genome Atlas (TCGA) cohort [58], *CD24* is significantly upregulated in *IDH1* and *IDH2* mutant (n = 410) relative to IDH wild-type (n = 94) tumors (**Fig. 1A**). *CD24* is similarly upregulated in IDH-mutant (n = 11) relative to wild-type (n = 141) GBMs from the TCGA (**Fig. 1B**). Differential gene expression analysis was carried out for the IDH mutant LGGs and showed significant differences in expression of many genes between $CD24^{high}$ (top quartile *CD24* expression, n = 103) and $CD24^{low}$ (bottom quartile, n = 103) tumors (**Fig. 1C, S1A**). Gene set enrichment analysis (GSEA) using the Hallmark gene set collection from the Molecular Signatures Database (MSigDB) revealed enrichment of MYC targets and cell cycle-associated programs in $CD24^{high}$ tumors (**Fig. 1D**). In addition, pathway enrichment analysis using the Reactome, Gene Ontology, and KEGG collections all pointed to neuronal signaling and ion channel activity as being overrepresented in $CD24^{low}$ tumors (**Fig. 1E, S1B and S1C**). GSEA was then performed again, this time with multiple MSigDB collections. This broader analysis confirmed that stem cell-related pathways are enriched in $CD24^{high}$ tumors, while markers of differentiated cell fates (neuronal and glial lineages) and neuronal signaling are enriched in $CD24^{low}$ tumors (**Fig. 1F, Tables S1, S2**).

Next, we examined the transcriptional profiles of two *IDH1* mutant models. The two cell models—the glioma tumorsphere line TS603 and an immortalized human neural stem cell (hNSC) line expressing ectopic $IDH1^{R132H}$ and *TERT*—were sorted by fluorescence-activated cell sorting (FACS) for CD24 expression. $CD24^+$ and $CD24^-$ populations, as well as an unsorted control (bulk cell line) were subjected to RNA sequencing (RNAseq). The CD24 transcriptional profile of the TS603 cell line (**Supplementary Fig. S1D**) is consistent with the TCGA data, with gene sets related to stem cells enriched in $CD24^+$ cells, and differentiation and neuronal pathways enriched in the $CD24^-$ subpopulation (**Fig. 2A-2C, S1E, S1F, Tables S1, S2**). $CD24^+$ *IDH1* mutant hNSCs (**Supplementary Fig. S2A and S2B**) also upregulate stem cell gene sets (**Fig. 2D-2F, S2C, S2D, Tables S1, S2**). Unsurprisingly, few gene sets indicative of differentiation were enriched in the hNSCs, irrespective of CD24 status (**Fig. 2D, Tables S1, S2**).

$CD24^+$ cells display increased stemness and proliferation rates in vitro

After separation of $CD24^+$ and $CD24^-$ TS603 cells by FACS, we examined the appearance and behavior of the cells. $CD24^-$ cells had an adherent phenotype more typical of differentiating neurospheres (**Fig. 3A**). Aside from the absence of $CD24^+$ cells, culture conditions were otherwise unchanged (Neurocult medium containing epidermal growth factor [EGF] and basic fibroblast growth factor [bFGF] for the maintenance of stem-like cells) [59–61]. A transwell assay, in which $CD24^-$ and $CD24^+$ cells were co-cultured on opposite sides of a membrane with 0.4 µm diameter pores, had no effect on the adherence of $CD24^-$ cells (data not shown). The 0.4 µm pores permit the flow of soluble factors and extracellular vesicles but block cell-cell contact.

$CD24^-$ TS603 cells demonstrated higher colony forming ability compared to their $CD24^+$ counterparts (**Fig. 3B**). $CD24^-$ clones also exhibited an adherent growth phenotype and an intermediate phenotype in which adherent cells, attached neurospheres, and rare floating neurospheres were concurrently present (**Fig. 3C and 3D**). We determined that 34.5% of $CD24^-$ clonal lines stopped dividing within a few passages (**Fig. 3D**). Conversely, only 8.3% of $CD24^+$ single-cell clones failed to continue to grow (**Fig. 3D**). $CD24^+$ clones all grew as unattached neurospheres (**Fig. 3D**), while unattached neurospheres comprised only 41.7% of $CD24^-$ clones (**Fig. 3D**).

Stem-like populations can exist in a balance with other cell types in a heterogeneous tumor cell population. Self-renewing cells were analyzed by flow cytometry to assess the stability of CD24 expression among individual clones. Clonal lines derived from both $CD24^+$ and $CD24^-$ cells demonstrated some degree of drift (**Fig. 3E**). The most significant plasticity was observed among $CD24^-$ clones; the unattached neurosphere growth phenotype in particular was most strongly associated with recovery of the $CD24^+$ cell compartment (**Fig. 3E**).

EdU incorporation assays show that the $CD24^+$ subgroup possess increased DNA synthesis frequency, which reflects proliferation rate (**Fig. 3F, S2E**). The increased proliferation rate of $CD24^+$ cells and the inherent plasticity of $CD24^-$ cells may help explain why $CD24^-$ sorted cells can progressively revert to a mixed $CD24^+/CD24^-$ population (**Fig. 3G**) and unsorted TS603 cells drift steadily in culture until they reach a primarily (>90%) $CD24^+$ state (**Supplementary Fig. S2F**). Together, these

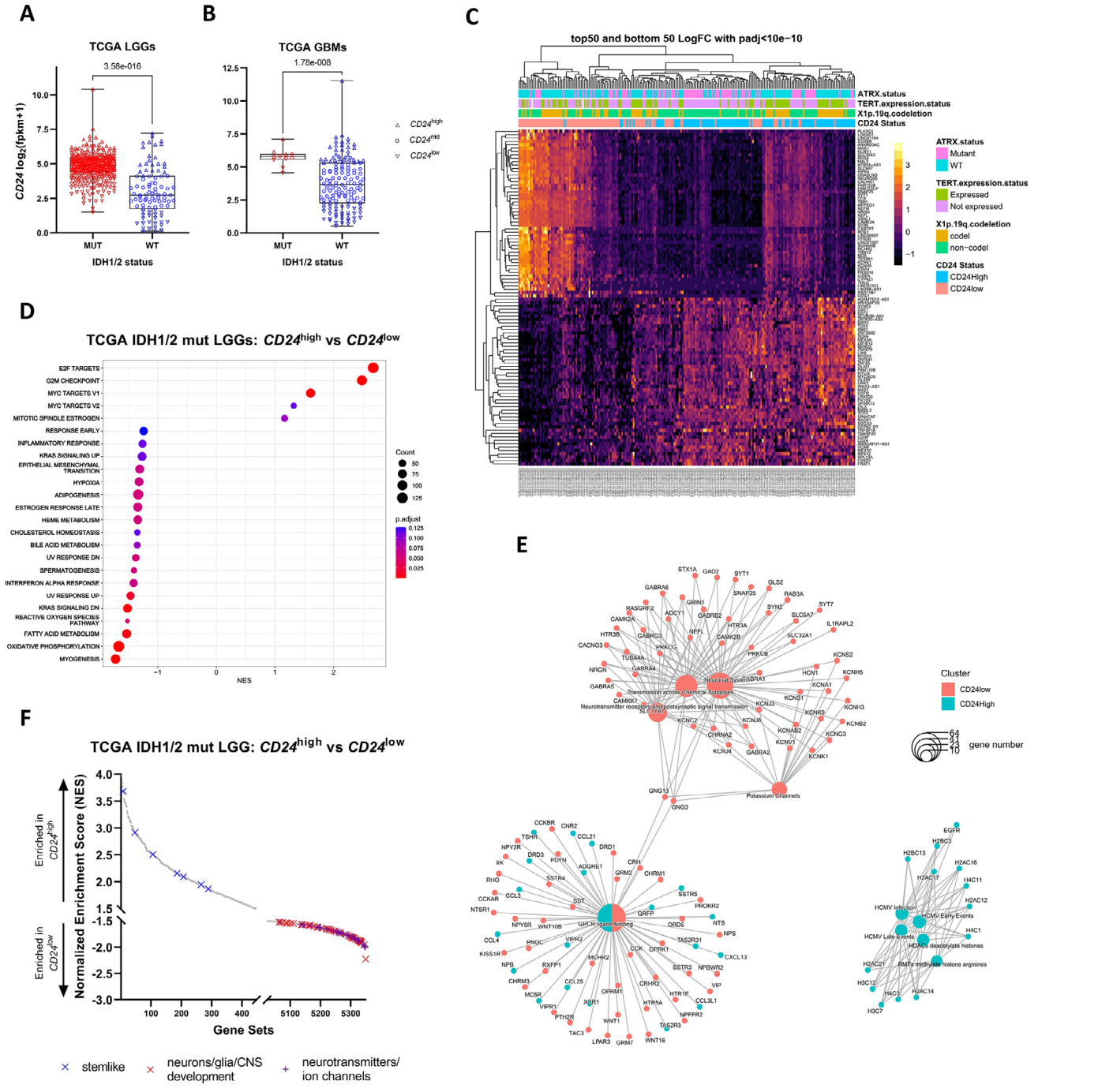

Fig. 1. Differential gene expression analysis reveals association between CD24 expression and stem cell associated transcriptional programs in LGG tumors. (**A**) and (**B**) CD24 expression is enriched in IDH mutant gliomas. Box-and-whisker plots showing *CD24* expression levels in *IDH1* and *IDH2* mutant versus wild-type LGGs (**A**) and GBMs (**B**) in the TCGA glioma data set. P value is indicated (Welch's t-test). Fpkm = Fragments per kilobase of transcript per million mapped reads (**C**) Hierarchical clustering of the top 50 upregulated and downregulated genes between $CD24^{high}$ and $CD24^{low}$ IDH-mutant LGGs reveals that CD24 status is associated with a distinct gene expression pattern. Top genes were selected by greatest $\log_2$ fold change, with an adjusted p value cutoff of $10e^{-10}$. (**D**) Dot plot representing GSEA using the Hallmark gene set collection, comparing $CD24^{high}$ and $CD24^{low}$ IDH-mutant LGGs. (**E**) Network plots showing differential pathway enrichment between $CD24^{high}$ and $CD24^{low}$ IDH mutant LGGs among the Reactome gene set collection. (**F**) Waterfall plots representing GSEA of RNAseq data of $CD24^{high}$ versus $CD24^{low}$ LGGs from the TCGA cohort. GSEA demonstrates enrichment of stem cell-associated molecular signatures in $CD24^{high}$ tumors, and enrichment of differentiation-associated signatures in $CD24^{low}$ tumors. A normalized enrichment score (NES) cutoff of +/- 1.5 was used. All gene sets shown have a false discovery rate (FDR) less than 0.1. Categories: stemlike (n=7), neurons/glia/CNS development (n=50), neurotransmitters/ion channels (n=50).

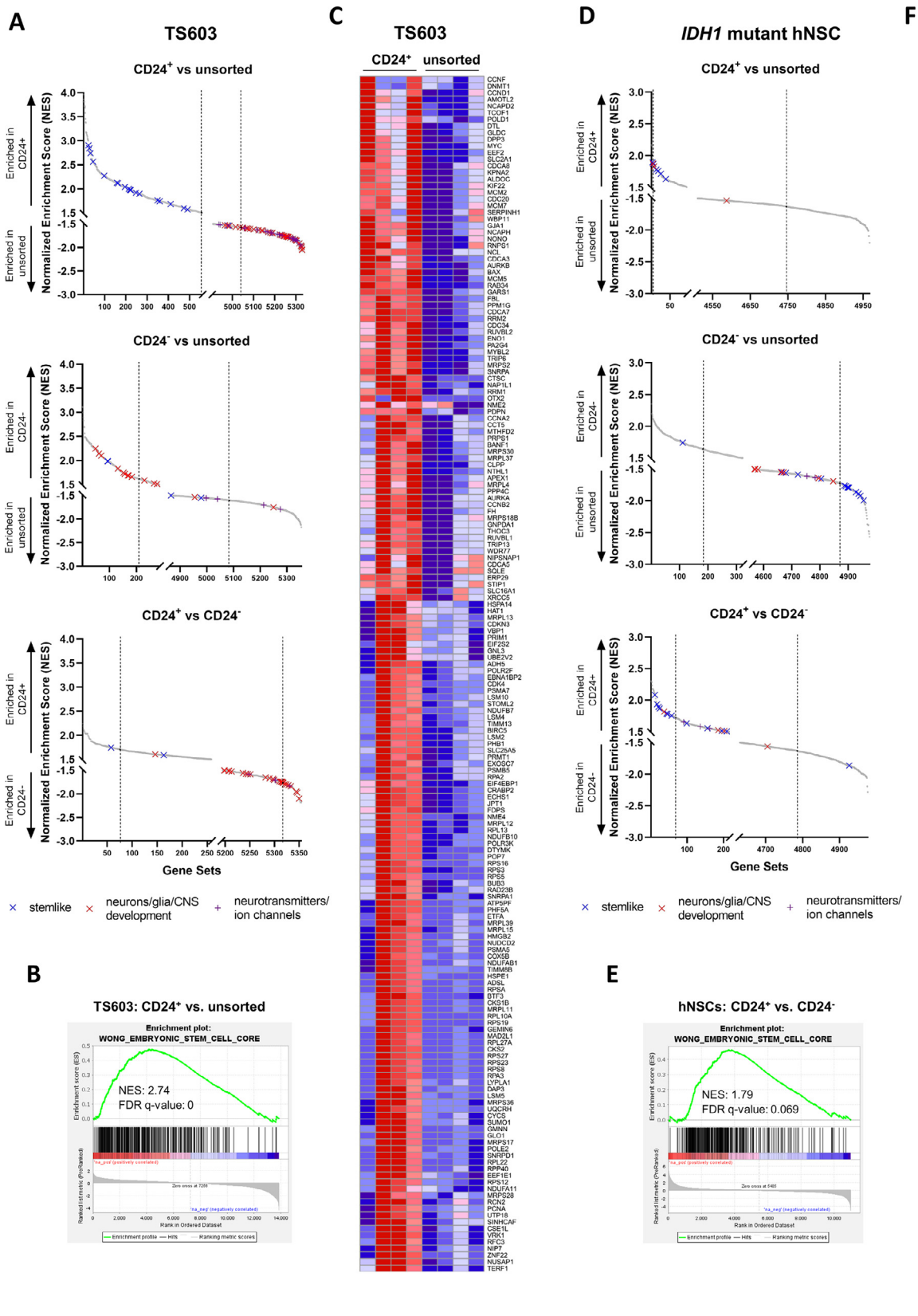

Fig. 2. CD24-expressing subpopulations in both glioma tumor cells and a hNSC model of IDH1-mutant glioma upregulate similar stem-like transcriptional programs. (**A**) GSEA of RNAseq data from the TS603 glioma tumorsphere line demonstrates enrichment of stem cell-associated molecular signatures in $CD24^+$ cells, and enrichment of differentiation-associated signatures in $CD24^-$ cells. NES cutoff of +/- 1.5 was used. Broken lines represent FDR < 0.1. *Top panel:* comparison of $CD24^+$ versus unsorted cells. Categories: stemlike (n=19), neurons/glia/CNS development (n=44),

observations are consistent with the presence of at least two phenotypic states that establish a balance in culture, similar to other cancer stem-associated populations.

To interrogate the differentiation capacity of CD24-sorted cells, cells were grown for 12 days in differentiation medium (containing serum) or serum-free proliferation medium (containing EGF and bFGF) on a growth factor-reduced Matrigel coating. In pro-differentiation conditions, $CD24^+$ cells maintained a more rounded shape, similar to undifferentiated cells (**Fig. 3H**). In proliferation medium, $CD24^-$ cells on Matrigel displayed a more differentiated appearance despite the presence of glioma stem cell-promoting growth factors (**Fig. 3H**); this is consistent with their adherence to uncoated tissue culture plastic after sorting (**Fig. 3A**). $CD24^-$ cells were quite heterogeneous in these conditions, but were generally astrocyte-like and process-bearing, with some flat, star-shaped cells also present (**Fig. 3H**). In differentiation medium, CD24- cells exhibited marked morphological changes, forming long, thin axon-like processes reminiscent of fusiform and multipolar neurons (**Fig. 3H**).

Gene expression analysis indicates that astrocytic lineage-like cells predominate amongst differentiated cells regardless of CD24 status, but that differentiation occurs to a much lesser extent in $CD24^+$ cells compared to $CD24^-$ cells. Differentiated $CD24^-$ cells upregulated the astrocytic lineage marker *GFAP* significantly more than $CD24^+$ cells and the unsorted (bulk cell line) control (**Fig. 3I**). Expression of astrocyte marker *AQP4* also consistently trended higher in $CD24^-$ cells (**Fig. 3I**). The parallel experiment using proliferation medium demonstrated no significant change in *GFAP* or *AQP4* expression over the 12-day time period under normal growth conditions that maintain undifferentiated stem cells (**Fig. 3I**).

CD24 is associated with differential tumor forming capacity in an orthotopic xenograft model

$CD24^+$, $CD24^-$, and unsorted TS603 cells were implanted intracranially into the forebrains of NOD-*scid* IL2Rγ^{null} (NSG) mice in serial dilutions ranging from 100,000 to 20 cells per animal. $CD24^+$ and unsorted cells were able to seed xenografts down to a minimum of 20 cells injected (**Fig. 4A**). Tumor initiation capacity of $CD24^-$ cells was significantly lower at 100 cells per injection, and completely abolished at 20 cells (**Fig. 4A**). In every case, tumors derived from $CD24^-$ cells exhibited slower growth and permitted longer survival versus $CD24^+$ cells (**Fig. 4B, S2G, S2H**).

Tumors were examined by two pathologists (Dr. Tejus Bale, Dr. Sebastien Monette, MSKCC) and they noted that all tumors possessed features similar to anaplastic oligodendroglioma. The three experimental groups (n = 5 tumors per group) appeared histologically similar except for the notable finding of abundant multinucleation and monstrocellular changes in 5 out of 5 tumors derived from $CD24^-$ cells (**Supplementary Fig. S3A and S3B**).

Immunofluorescent staining of tumor sections derived from injection of TS603 cells revealed that CD24-expressing cells and CD24 negative cells are heterogeneously distributed, with $CD24^+$ cells enriched in necrotic regions (**Fig. 4C, S3C**). $CD24^-$ tumors exhibited strikingly higher expression of S100B (**Fig. 4D and 4E**), a marker of astrocytic differentiation. Immunofluorescent staining was quantified using a custom ImageJ script (**Fig. 4E, S3D**), which captured a more subtle enrichment of Olig2 and Sox2 in $CD24^-$ tumors.

Unexpectedly, no tumors in this study were positive for GFAP. Staining of other markers, including Ki-67, CD31, Iba1, PD-L1, and nestin (**Fig. 4E, S3E**), did not reveal significant differences between the three groups.

Consequences of CD24 *depletion on cell viability, proliferation and gene expression* in vitro

Constitutively expressed shRNAs targeting *CD24* caused cell death in the vast majority of TS603 cells, with no toxicity noted from the nontargeting control (NTC) cells (data not shown). After several weeks, the resistant, surviving cells harboring the sh*CD24* expanded into a predominantly $CD24^+$ population (**Fig. 5A**). Expression of the bacterial gene *pac*, which confers resistance to puromycin, was confirmed by qRT-PCR (**Supplementary Fig. S3F**), indicating that the survivors were successfully transduced with the pLKO.1-puro (Addgene #8453) shRNA vector. Because strong constitutive depletion of CD24 appears to result in cell death, the short hairpins were cloned into a doxycycline (dox)-inducible construct, and the dose of dox was titrated to allow for knockdown of CD24 (**Fig. 5B, S3G**), while permitting cell survival. At 100 ng/mL dox, expression of anti-*CD24* shRNAs resulted in a reduction of proliferation rate as measured by EdU assay (**Fig. 5C**).

A representative panel of genes upregulated in $CD24^-$ sorted TS603 cells were selected from RNAseq data to represent markers of the astroglial (*AQP4, GFAP*, and *S100B*), oligodendroglial (*OLIG1* and *OLIG2*), and neuronal (*MAP2* and *NEUROD1*) lineages; the neural stem cell markers *SOX2* and *NES* were also included in the panel (**Fig. 5D**). Anti-*CD24* shRNA-mediated knockdown (under dox-induced hairpin expression) resulted in expression levels that mirrored those in the naturally occurring $CD24^-$ cells (**Fig. 5E**).

Although *CD24* knockdown induced a baseline upregulation of differentiation markers similar to $CD24^-$ cells, the *in vitro* differentiation capacity as measured by differentiation markers was not significantly different from cells expressing the nontargeting control (**Fig. 5F**). To determine if *CD24* knockdown could affect tumor initiation capacity or tumor aggressiveness, cells expressing inducible sh*CD24* and control shRNA were implanted intracranially into NSG mice fed dox-containing chow. Survival was not significantly different between the three groups (**Fig. 5G**). These data suggest that CD24 is a marker for a stem-like tumor cell population that is induced by mutant IDH and that it can promote the acquisition of features that help drive tumor progression but alone may not be sufficient to alter *in vivo* tumor growth kinetics.

Overexpression of CD24 *alone in glioma tumor cells is not sufficient to enhance stem-like behavior*

We overexpressed CD24 in TS603 glioma tumorsphere cells. qRT-PCR and flow cytometry confirmed that these cells indeed overexpressed CD24

neurotransmitters/ion channels (n=28). *Center panel:* comparison of $CD24^-$ versus unsorted cells. Categories: stemlike (n=4), neurons/glia/CNS development (n=14), neurotransmitters/ion channels (n=4). *Bottom panel:* comparison of $CD24^+$ versus $CD24^-$ cells. Categories: stemlike (n=2), neurons/glia/CNS development (n=27), neurotransmitters/ion channels (n=4). (**B**) GSEA enrichment plot showing that gene expression profiles associated with embryonic stem cells are significantly upregulated in $CD24^+$ as compared to unsorted TS603 glioma cells. (**C**) Heatmap for the leading edge subset of genes that contribute the most to the enrichment score shown in (B).(**D**) GSEA of RNAseq data from *IDH1* mutant hNSCs demonstrates enrichment of stem cell-associated molecular signatures in $CD24^+$ cells. NES cutoff of +/- 1.5 was used. Broken lines represent FDR < 0.1. *Top panel:* comparison of $CD24^+$ versus unsorted cells. Categories: stemlike (n=6), neurons/glia/CNS development (n=3), neurotransmitters/ion channels (n=0). *Center panel:* comparison of $CD24^-$ versus unsorted cells. Categories: stemlike (n=14), neurons/glia/CNS development (n=7), neurotransmitters/ion channels (n=2). *Bottom panel:* comparison of $CD24^+$ versus $CD24^-$ cells. Categories: stemlike (n=12), neurons/glia/CNS development (n=4), neurotransmitters/ion channels (n=3). (**E**) GSEA enrichment plot showing that gene expression profiles associated with embryonic stem cells are significantly upregulated in $CD24^+$ as compared to $CD24^-$ hNSCs. (**F**) Heatmap for the leading edge subset of genes that contribute the most to the enrichment score shown in (E).

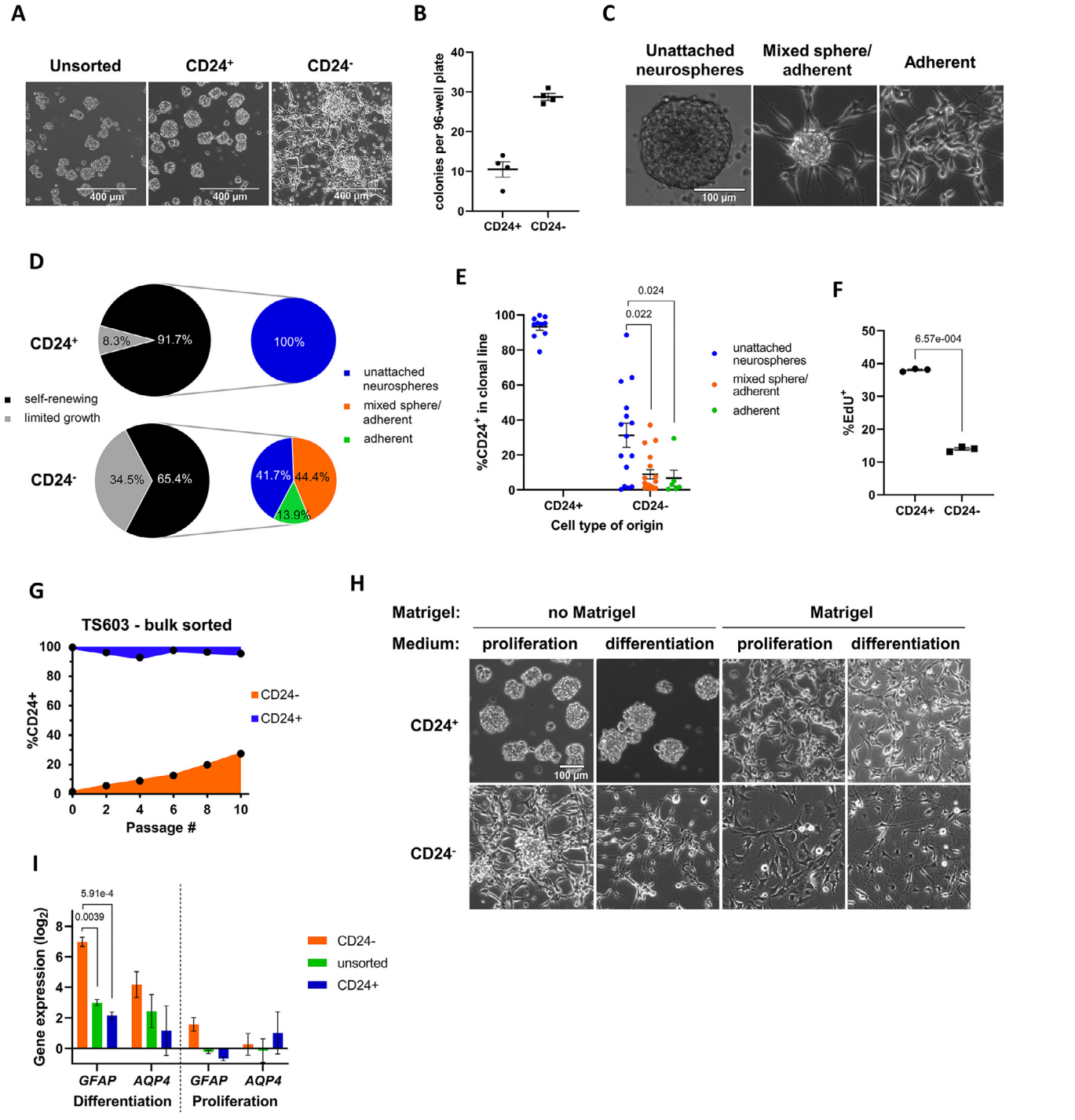

Fig. 3. CD24 expression in glioma tumor cells is associated with stem-like phenotypes *in vitro*. (**A**) Representative brightfield images showing phenotypic differences between $CD24^+$ and $CD24^-$ sorted TS603 glioma cells. (**B**) Total clonal viability of $CD24^+$ and $CD24^-$ TS603 cells sorted by FACS, 1 cell per well. Error bars = standard error of the mean (SEM). (**C**) Representative brightfield images of the three growth phenotypes observed in clonal lines derived from the TS603 cell line. (**D**) Phenotypes observed in clonal lines derived from $CD24^+$ and $CD24^-$ TS603 cells. Self-renewing clones from each group are subdivided by growth phenotypes. (**E**) Percentage of $CD24^+$ cells in self-renewing clonal lines measured by flow cytometry, grouped by phenotype. Significant p values are indicated (Welch's ANOVA with Dunnett's T3 multiple comparisons test). Error bars = SEM. (**F**) EdU incorporation assay measuring DNA synthesis in proliferating TS603 cells. P value is indicated (paired t-test). Error bars = SEM. (**G**) Reversion of bulk-sorted $CD24^+$ and $CD24^-$ TS603 cells to a mixed population. Percentage of $CD24^+$ cells in sorted cell populations was measured over time by flow cytometry. Reversion occurs primarily in $CD24^-$ sorted cells. (**H**) Representative brightfield images showing cellular morphologies of $CD24^+$ and $CD24^-$ TS603 cells in standard growth (proliferation) medium and differentiation medium, with and without a coating of growth factor-reduced Matrigel. The first column of (H) is a duplication of (A), included for clarity. (**I**) qRT-PCR measuring expression of astrocytic markers *GFAP* and *AQP4* in TS603 cells grown on growth factor-reduced Matrigel in differentiation medium or proliferation medium. Y axis is $\log_2$ fold gene expression at endpoint (day 12) versus baseline (day 0). Significant p-values are indicated (Welch's ANOVA with Dunnett's T3 multiple comparisons test). Error bars = SEM.

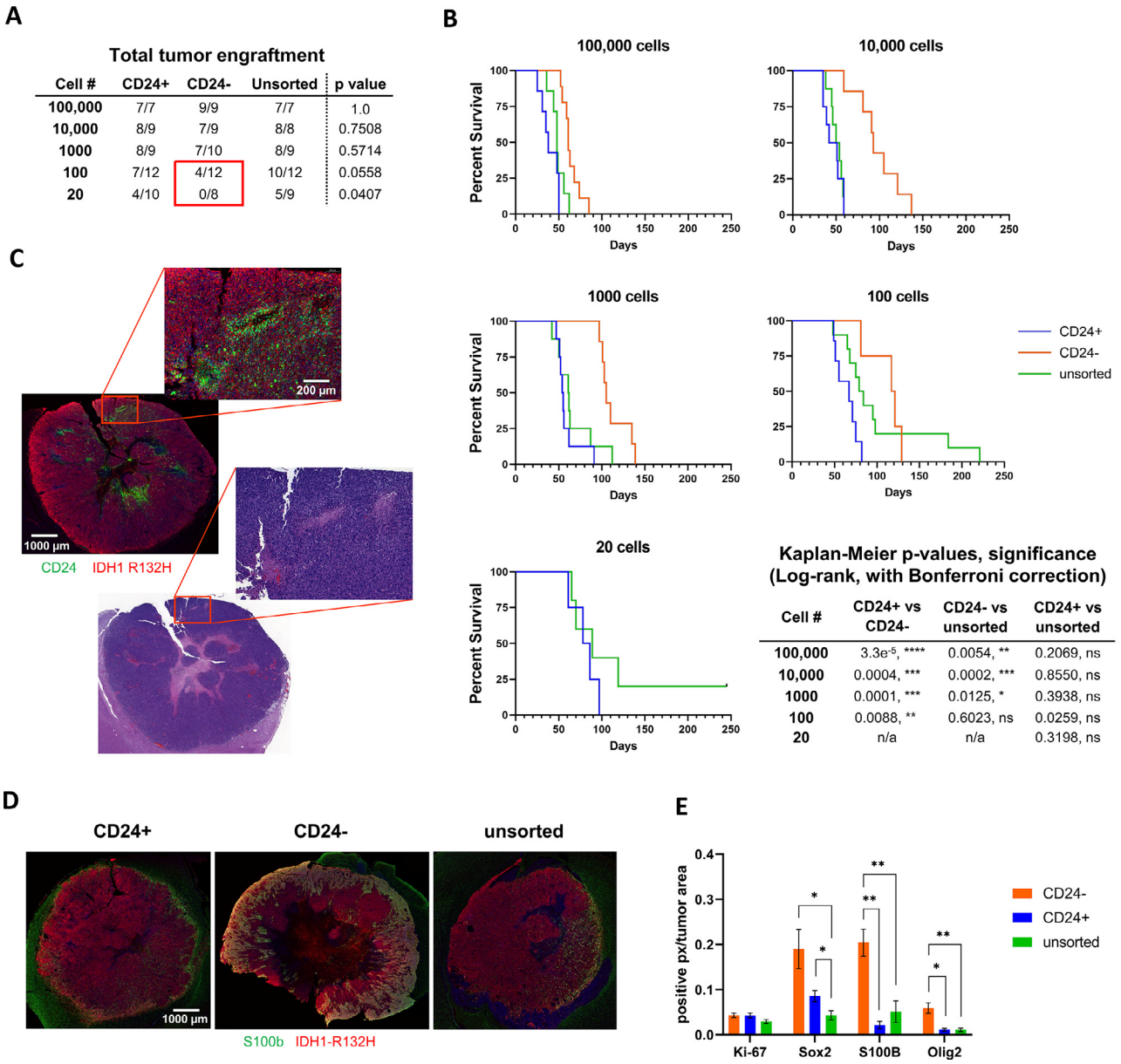

Fig. 4. CD24$^+$ cells have greater tumor initiation ability. (**A**) Total tumor engraftment of TS603 cells intracranially injected into NSG mice. P values were determined by a Fisher-Freeman-Halton test. Red box: tumor initiation capacity of CD24$^-$ cells is reduced at 100 cells injected, and abolished at 20 cells. (**B**) Kaplan-Meier survival curves of tumor-bearing mice. P values are indicated in table (bottom right). (**C**) Representative images showing CD24 staining near necrotic areas. Top: immunofluorescence; IDH1-R132H stains all tumor cells. Bottom: H+E stain of the same tumor section. (**D**) Representative images showing increased S100B staining in xenograft tumors derived from CD24$^-$ TS603 cells. S100B antibody is human/mouse cross-reactive; murine astrocytes are also stained in green. IDH1-R132H serves as a marker of tumor cells. (**E**) Results of quantitation of immunofluorescent images of xenograft tumors. Y axis is number of positive pixels / total area of tumor section, determined by expression of mutant IDH1 protein above an optimized threshold brightness level. (Quantitation strategy described in methods.) N = 5 tumors per group. Significant p values (Welch's ANOVA with Dunnett's T3 multiple comparisons test) are represented as follows: **, $0.001 < p \leq 0.01$; *, $0.01 < p \leq 0.05$. Error bars = SEM.

(Fig. 6A, S3H). Overexpression (OE) of *CD24* alone in the tumor cells did not induce further changes in the expression level of differentiation-associated genes or proliferation rate (Fig. 6B and 6C). *CD24* was overexpressed in the unsorted cell line and in CD24$^-$ sorted cells (Fig. 6A) with similar results. Tumor cells overexpressing CD24 had similar tumor initiating capabilities to the vector control, and no significant differences in survival were observed between the two groups (Fig. 6D). Immunofluorescent staining of xenograft tumors (Fig. 6E, S3I) revealed a modest increase in Ki-67 staining in CD24 OE tumors. Together, these data show that CD24, by itself, is not sufficient to result in further enhancement of stem-like properties in tumor cells. CD24$^+$ therefore marks and helps promote stem-like features and tumorigenesis but other CD24-independent processes are likely also needed in establishing stem-like phenotypes.

Discussion

The acquisition of stem cell-like features is recognized as a critical aspect of glioma biology [62–65]. The development of aberrant *CD24* expressing cells is one consequence of the sweeping phenotypic reprogramming induced by *IDH1* mutation. CD24 is recognized as a marker of stem-like cell populations

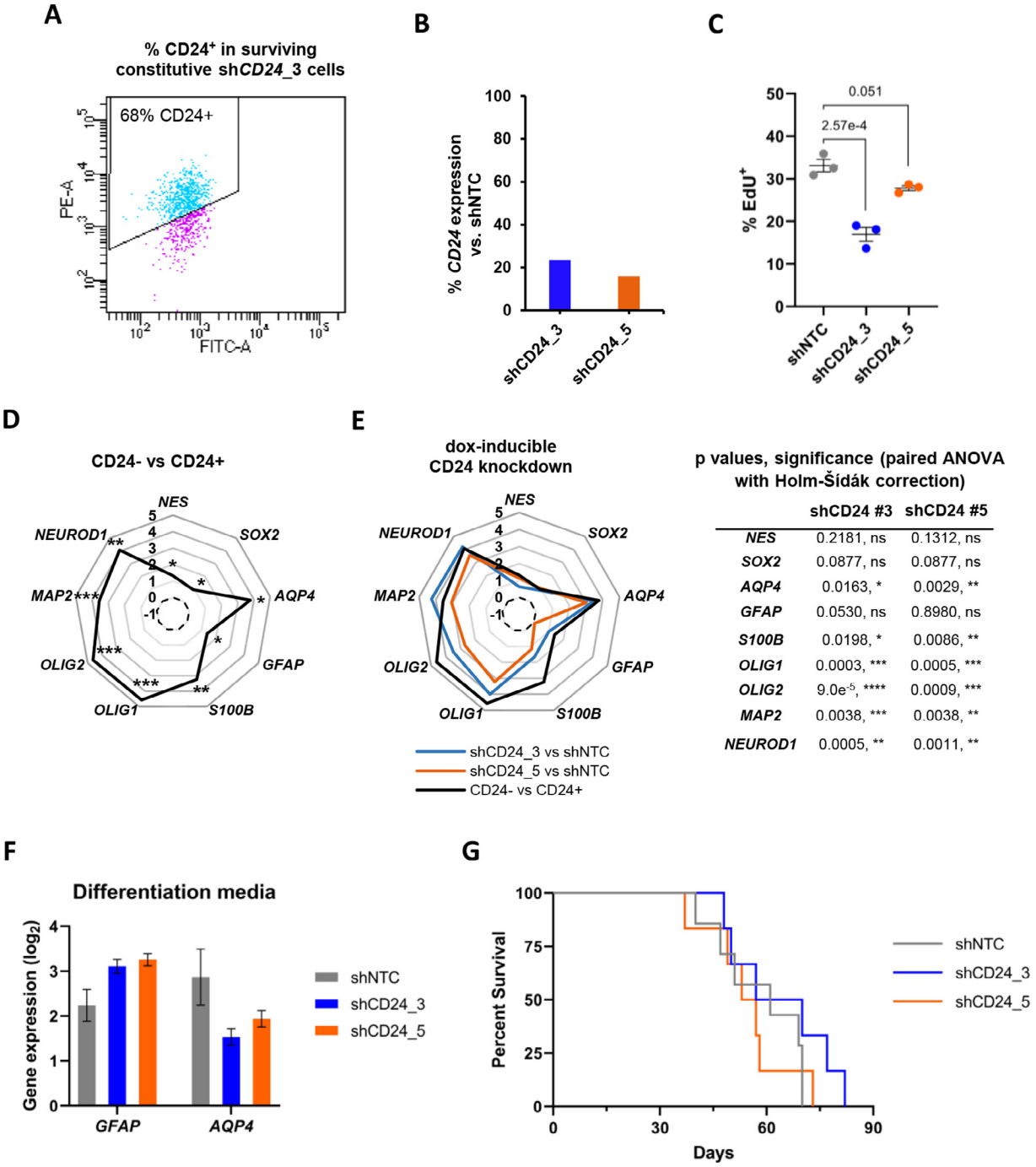

Fig. 5. ***CD24*** **depletion impacts viability, gene expression and proliferation in glioma tumorsphere cells.** (**A**) Representative flow cytometry plot showing a high percentage of $CD24^+$ cells in surviving cells harboring constitutively expressed sh*CD24*. (**B**) qRT-PCR of TS603 cells harboring dox-inducible sh*CD24* and shNTC. The medium was supplemented with a final concentration of 100 ng/mL dox to induce *CD24* knockdown. (**C**) EdU incorporation assay measuring DNA synthesis in proliferating TS603 cells harboring dox-inducible sh*CD24* and shNTC. P values are indicated (one-way ANOVA with Dunnett's multiple comparisons test). Error bars = SEM. (**D**) Panel of differentiation and stem markers selected from RNA-seq of CD24-sorted TS603 cells, displayed as a radar plot. Y axes are $\log_2$ fold gene expression. Black broken line at $\log_2$ gene expression = 0. P values are represented as follows: ***, $p < 1e^{-100}$; **, $1e^{-100} \leq p < 1e^{-50}$; *, $1e^{-50} \leq p < 1e^{-08}$ (calculated by DeSeq2 using the Benjamini-Hochberg correction). (**E**) Radar plot of qRT-PCR data from TS603 cells harboring dox-inducible sh*CD24* relative to shNTC. The RNAseq data from (D) is overlayed with the shRNA data. Y axes are $\log_2$ fold gene expression relative to shNTC. Black broken line at $\log_2$ gene expression = 0. P values are indicated in table (right). (**F**) qRT-PCR measuring expression of astrocytic markers *GFAP* and *AQP4* in TS603 cells harboring sh*CD24* or shNTC, grown in differentiation conditions. Y axis is $\log_2$ fold gene expression at endpoint (day 12) versus baseline (day 0). Error bars = SEM. P values not significant (Welch's ANOVA with Dunnett's T3 multiple comparisons test). (**G**) Kaplan-Meier curves showing survival of mice harboring tumors expressing dox-inducible shCD24 (sh*CD24* #3, n = 6; sh*CD24* #5, n = 6) and shNTC (n = 7). 5000 cells were injected per animal. Log-rank p-values not significant.

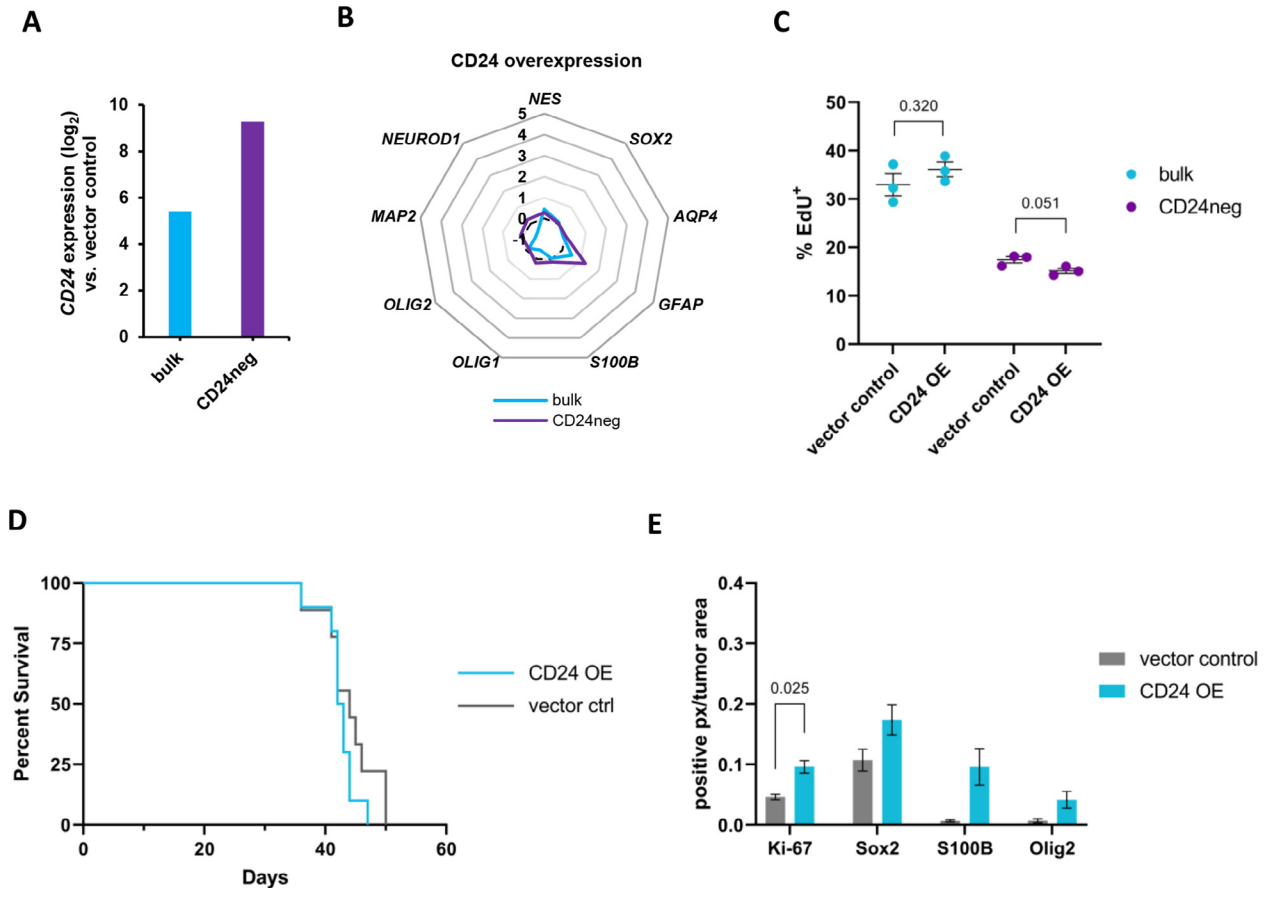

Fig. 6. Overexpression of CD24 alone is not sufficient to recapitulate CD24$^+$ phenotypes in TS603 glioma cells. (**A**) qRT-PCR of TS603 cells harboring the CD24 overexpression construct and empty vector control. Both CD24$^-$ and unsorted (bulk) TS603 cells were transduced with the overexpression and control vectors. (**B**) Radar plot of qRT-PCR data from TS603 cells harboring the CD24 overexpression construct relative to empty vector control. Y axes are $\log_2$ fold gene expression relative to the vector control. Black broken line at $\log_2$ gene expression = 0. P values not significant (paired t-tests with Holm-Šídák correction). (**C**) EdU incorporation assay measuring DNA synthesis in proliferating TS603 cells harboring CD24 overexpression construct and empty vector control. P values are indicated (Welch's t-test). Error bars = SEM. (**D**) Kaplan-Meier curves showing survival of mice harboring tumors expressing the CD24 overexpression construct (n = 10) and empty vector control (n = 9). 5000 cells were injected per animal. Log-rank p-value = 0.2058 (ns). (**E**) Quantitation of immunofluorescent images of xenograft tumors. Y axis is number of positive pixels / total area of tumor section, determined by expression of mutant IDH1 protein above an optimized threshold brightness level. (Quantitation strategy described in methods.) N = 3 tumors per group. Significant p-value is indicated (Welch's t-test). Error bars = SEM.

in a number of different malignancies. Here, we demonstrate that CD24 strongly associates with stemness and enhanced tumorigenicity in *IDH1* mutant gliomas and reveal distinctive molecular features associated with the CD24$^+$ tumor cell population. Moreover, CD24 plays a role, along with other factors, to maintain stemness.

Transcriptome analysis of IDH1 mutant TS603 glioma tumorsphere cells and TCGA data show distinct molecular differences between CD24$^+$/*CD24*^{high} and CD24$^-$/*CD24*^{low} cells in relation to gene expression patterns, stem cell-associated transcriptional programs, and capacity for differentiation. Similar to the TS603s, *TERT*-immortalized hNSCs expressing mutant *IDH1* upregulate stemness programs in the CD24$^+$ compartment.

CD24$^+$ TS603 cells grow as unattached neurospheres, typical of stem-like cells, and can, in part, resist differentiating. It appears that CD24$^-$ cells are similar to a type of intermediate or transit-amplifying state that is more poised for differentiation. Clonal lines derived from CD24$^-$ cells demonstrate more limited growth potential and reduced sphere formation capacity, and exhibit an adherent growth phenotype not seen in CD24$^+$ cells.

CD24$^-$ cells upregulate markers of glial and neuronal differentiation at baseline. Once separated from CD24$^+$ cells by FACS, CD24$^-$ cells differentiate, even in stem cell medium supplemented with EGF and bFGF. Co-culturing in a transwell failed to rescue this phenotype, indicating that CD24$^+$ cells do not influence the differentiation state of their CD24$^-$ counterparts using only secreted factors, but rather, at least in part, through juxtacrine signaling mediated by direct cell-cell contact.

Our limiting dilution tumorigenesis studies revealed that CD24$^+$ TS603 cells are more efficient at forming tumors and produce more aggressive tumors compared to CD24$^-$ cells. Localization of CD24$^+$ tumor cells in the peri-necrotic niche is consistent with what is seen by others examining the location of cancer stem cells [67,68]. This localization is also consistent with previous work showing that *CD24* expression is associated with hypoxia [66]. These histologic features imply that CD24$^+$ cells are located in aggressive areas of the tumor that are growing rapidly.

Both CD24$^+$ and CD24$^-$ TS603 cells produce mostly CD24-negative tumors, but only tumors derived from CD24$^-$ cells upregulate S100B. It is important to note that the CD24-negative cells within the three cohorts of xenograft tumors have not necessarily differentiated to the same extent. The differentiation of neural stem cells is a stepwise process that passes through several intermediate stages before terminal differentiation [67–69], and in a similar fashion, glioma tumor cells can also exist on a spectrum from

stem-like to more differentiated. Mutant IDH promotes an aberrant stem-like state by blocking differentiation [12]; however, IDH-mutant tumors are heterogeneous and not uniformly stem-like. It stands to reason that some tumor cells would be "blocked" at a later stage than others, allowing for varying degrees of differentiation *in vivo*. We have shown that $CD24^-$ cells are in a "poised" state, already steps ahead of $CD24^+$ cells on the path to differentiation. $CD24^+$ cells can differentiate *in vitro* when EGF/bFGF are removed and serum is added, but they do so to a lesser degree than $CD24^-$ cells. The loss of CD24 is perhaps an early event in the differentiation process, and the induction of S100B—a marker of the mature astrocytic lineage—is a late one [70].

Dox-controlled *CD24* knockdown with inducible shRNA induced gene expression and proliferative changes that recapitulate a "$CD24^-$-like" phenotype *in vitro*. This strongly implicates CD24 itself in helping to maintain some of the phenotypes we observed. It is possible that the approximately 80% *CD24* knockdown achievable with 100 ng/mL dox (**Fig. 5B**) allowed the cells to survive but may have been insufficient to induce statistically significant changes when cells were grown in pro-differentiation conditions.

In our *in vitro* studies, we had observed that anti-*CD24* shRNAs are cytotoxic when expressed constitutively, and selective pressure in resistant cells strongly favors the silencing of hairpin expression. *CD24* knockdown may be similarly selected against *in vivo* if CD24 promotes cell survival in the brain as well as in culture. Overexpression of CD24 did not confer an enhanced stem-like phenotype in TS603 tumor cells, suggesting that CD24 is one factor that is required to maintain—but not induce—stemness. Maintenance of stemness via CD24 signaling likely requires another protein that is not expressed in $CD24^-$ cells. Previously reported CD24 interactors include Src family kinases [71–74], P-selectin [75], E-selectin [76], Siglec-5 [42] and Siglec-10 [42,75–77]. The elucidation of the rest of the CD24 signaling pathway will be an important avenue for future investigation.

Data availability

Genomics data from this study are deposited at Sequence Read Archive (SRA).

Financial Support

This research was funded by the National Institutes of Health, R01CA205426 and R35CA232097 (TAC).

Author Contributions

Conceptualization, S.H., S.T, T.A.C.; Methodology, S.H., S.T., T.A.C.; Investigation, S.H., Y.W., W.W., T.B., S.M.; Formal Analysis, T.J.A., H.H., E.R., X.M., A.D., V.M.; Visualization, S.H., T.J.A, H.H.; Project Administration, R.G, K.M.; Writing – Original Draft, S.H.; Writing – Review & Editing, T.A.C.; Funding Acquisition, T.A.C.; Supervision, T.A.C, A.B.

Acknowledgements

We would like to thank colleagues at the MSK core facilities, including Integrated Genomics Operation (IGO), Flow Cytometry Core Facility (FCCF), Laboratory of Comparative Pathology (LCP) and Molecular Cytology Core Facility (MCCF) for processing our samples and providing important suggestions. We would like to thank all the members and alumni of the Chan lab for their generous help and support of this study. The results presented here are in part based upon data generated or collected by the TCGA Research Network: https://www.cancer.gov/tcga; Broad CCLE, https://portals.broadinstitute.org/ccle; ICGC, https://icgc.org/. We also acknowledge NIH Cancer Center Support Grant P30 CA008748, which supports MSKCC core facilities, and a Shared Resources Grant from the MSKCC Metastasis Research Center, which provided funding support for the purchase of the IVIS Spectrum.

Supplementary materials

Supplementary material associated with this article can be found, in the online version, at doi:10.1016/j.neo.2022.100790.

References

[1] Stupp R, Mason WP, van den Bent MJ, Weller M, Fisher B, Taphoorn MJB, Belanger K, Brandes AA, Marosi C, Bogdahn U, Curschmann J, Janzer RC, Ludwin SK, Gorlia T, Allgeier A, Lacombe D, Cairncross JG, Eisenhauer E, Mirimanoff ROEuropean Organisation for Research and Treatment of Cancer Brain Tumor and Radiotherapy Groups, National Cancer Institute of Canada Clinical Trials Group. Radiotherapy plus concomitant and adjuvant temozolomide for glioblastoma. *N Engl J Med* 2005;**352**:987–96. doi:10.1056/NEJMoa043330.

[2] Cahill DP. Extent of resection of glioblastoma: A critical evaluation in the molecular era. *Neurosurg Clin N Am* 2021;**32**:23–9. doi:10.1016/j.nec.2020.09.006.

[3] Ohgaki H, Kleihues P. The definition of primary and secondary glioblastoma. *Clin Cancer Res* 2013;**19**:764–72. doi:10.1158/1078-0432.CCR-12-3002.

[4] Miller JJ, Loebel F, Juratli TA, Tummala SS, Williams EA, Batchelor TT, Arrillaga-Romany I, Cahill DP. Accelerated progression of IDH mutant glioma after first recurrence. *Neuro Oncol* 2019;**21**:669–77. doi:10.1093/neuonc/noz016.

[5] Barthel FP, Johnson KC, Varn FS, Moskalik AD, Tanner G, Kocakavuk E, Anderson KJ, Abiola O, Aldape K, Alfaro KD, Alpar D, Amin SB, Ashley DM, Bandopadhayay P, Barnholtz-Sloan JS, Beroukhim R, Bock C, Brastianos PK, Brat DJ, Brodbelt AR, Consortium GLASS. Longitudinal molecular trajectories of diffuse glioma in adults. *Nature* 2019;**576**:112–20. doi:10.1038/s41586-019-1775-1.

[6] Jaeckle KA, Decker PA, Ballman KV, Flynn PJ, Giannini C, Scheithauer BW, Jenkins RB, Buckner JC. Transformation of low grade glioma and correlation with outcome: an NCCTG database analysis. *J Neurooncol* 2011;**104**:253–9. doi:10.1007/s11060-010-0476-2.

[7] Yan H, Parsons DW, Jin G, McLendon R, Rasheed BA, Yuan W, Kos I, Batinic-Haberle I, Jones S, Riggins GJ, Friedman H, Friedman A, Reardon D, Herndon J, Kinzler KW, Velculescu VE, Vogelstein B, Bigner DD. IDH1 and IDH2 mutations in gliomas. *N Engl J Med* 2009;**360**:765–73. doi:10.1056/NEJMoa0808710.

[8] Liu A, Hou C, Chen H, Zong X, Zong P. Genetics and epigenetics of glioblastoma: applications and overall incidence of IDH1 mutation. *Front Oncol* 2016;**6**:16. doi:10.3389/fonc.2016.00016.

[9] Parsons DW, Jones S, Zhang X, Lin JC-H, Leary RJ, Angenendt P, Mankoo P, Carter H, Siu I-M, Gallia GL, Olivi A, McLendon R, Rasheed BA, Keir S, Nikolskaya T, Nikolsky Y, Busam DA, Tekleab H, Diaz LA, Hartigan J, Kinzler KW. An integrated genomic analysis of human glioblastoma multiforme. *Science* 2008;**321**:1807–12. doi:10.1126/science.1164382.

[10] McKenney AS, Levine RL. Isocitrate dehydrogenase mutations in leukemia. *J Clin Invest* 2013;**123**:3672–7. doi:10.1172/JCI67266.

[11] Dang L, White DW, Gross S, Bennett BD, Bittinger MA, Driggers EM, Fantin VR, Jang HG, Jin S, Keenan MC, Marks KM, Prins RM, Ward PS, Yen KE, Liau LM, Rabinowitz JD, Cantley LC, Thompson CB, Vander Heiden MG, Su SM. Cancer-associated IDH1 mutations produce 2-hydroxyglutarate. *Nature* 2009;**462**:739–44. doi:10.1038/nature08617.

[12] Lu C, Ward PS, Kapoor GS, Rohle D, Turcan S, Abdel-Wahab O, Edwards CR, Khanin R, Figueroa ME, Melnick A, Wellen KE, O'Rourke DM, Berger SL, Chan TA, Levine RL, Mellinghoff IK, Thompson CB. IDH mutation impairs histone demethylation and results in a block to cell differentiation. *Nature* 2012;**483**:474–8. doi:10.1038/nature10860.

[13] Turcan S, Rohle D, Goenka A, Walsh LA, Fang F, Yilmaz E, Campos C, Fabius AWM, Lu C, Ward PS, Thompson CB, Kaufman A, Guryanova O, Levine R, Heguy A, Viale A, Morris LGT, Huse JT, Mellinghoff IK, Chan TA. IDH1 mutation is sufficient to establish the glioma hypermethylator phenotype. *Nature* 2012;**483**:479–83. doi:10.1038/nature10866.

[14] Flavahan WA, Drier Y, Liau BB, Gillespie SM, Venteicher AS, Stemmer-Rachamimov AO, Suvà ML, Bernstein BE. Insulator dysfunction and oncogene activation in IDH mutant gliomas. *Nature* 2016;**529**:110–14. doi:10.1038/nature16490.

[15] Figueroa ME, Abdel-Wahab O, Lu C, Ward PS, Patel J, Shih A, Li Y, Bhagwat N, Vasanthakumar A, Fernandez HF, Tallman MS, Sun Z, Wolniak K, Peeters JK, Liu W, Choe SE, Fantin VR, Paietta E, Löwenberg B, Licht JD, Melnick A. Leukemic IDH1 and IDH2 mutations result in a hypermethylation phenotype, disrupt TET2 function, and impair hematopoietic differentiation. *Cancer Cell* 2010;**18**:553–67. doi:10.1016/j.ccr.2010.11.015.

[16] Duncan CG, Barwick BG, Jin G, Rago C, Kapoor-Vazirani P, Powell DR, Chi J-T, Bigner DD, Vertino PM, Yan H. A heterozygous IDH1R132H/WT mutation induces genome-wide alterations in DNA methylation. *Genome Res* 2012;**22**:2339–55. doi:10.1101/gr.132738.111.

[17] Tirosh I, Venteicher AS, Hebert C, Escalante LE, Patel AP, Yizhak K, Fisher JM, Rodman C, Mount C, Filbin MG, Neftel C, Desai N, Nyman J, Izar B, Luo CC, Francis JM, Patel AA, Onozato ML, Riggi N, Livak KJ, Suvà ML. Single-cell RNA-seq supports a developmental hierarchy in human oligodendroglioma. *Nature* 2016;**539**:309–13. doi:10.1038/nature20123.

[18] Venteicher AS, Tirosh I, Hebert C, Yizhak K, Neftel C, Filbin MG, Hovestadt V, Escalante LE, Shaw ML, Rodman C, Gillespie SM, Dionne D, Luo CC, Ravichandran H, Mylvaganam R, Mount C, Onozato ML, Nahed BV, Wakimoto H, Curry WT, Suvà ML. Decoupling genetics, lineages, and microenvironment in IDH-mutant gliomas by single-cell RNA-seq. *Science* 2017:355. doi:10.1126/science.aai8478.

[19] Chaligne R, Gaiti F, Silverbush D, Schiffman JS, Weisman HR, Kluegel L, Gritsch S, Deochand SD, Gonzalez Castro LN, Richman AR, Klughammer J, Biancalani T, Muus C, Sheridan C, Alonso A, Izzo F, Park J, Rozenblatt-Rosen O, Regev A, Suvà ML, Landau DA. Epigenetic encoding, heritability and plasticity of glioma transcriptional cell states. *Nat Genet* 2021;**53**:1469–79. doi:10.1038/s41588-021-00927-7.

[20] Turcan S, Makarov V, Taranda J, Wang Y, Fabius AWM, Wu W, Zheng Y, El-Amine N, Haddock S, Nanjangud G, LeKaye HC, Brennan C, Cross J, Huse JT, Kelleher NL, Osten P, Thompson CB, Chan TA. Mutant-IDH1-dependent chromatin state reprogramming, reversibility, and persistence. *Nat Genet* 2018;**50**:62–72. doi:10.1038/s41588-017-0001-z.

[21] Tiburcio PDB, Locke MC, Bhaskara S, Chandrasekharan MB, Huang LE. The neural stem-cell marker CD24 is specifically upregulated in IDH-mutant glioma. *Transl. Oncol.* 2020;**13**:100819. doi:10.1016/j.tranon.2020.100819.

[22] Poncet C, Frances V, Gristina R, Scheiner C, Pellissier JF, Figarella-Branger D. CD24, a glycosylphosphatidylinositol-anchored molecules is transiently expressed during the development of human central nervous system and is a marker of human neural cell lineage tumors. *Acta Neuropathol* 1996;**91**:400–8. doi:10.1007/s004010050442.

[23] Senner V, Sturm A, Baur I, Schrell UH, Distel L, Paulus W. CD24 promotes invasion of glioma cells in vivo. *J Neuropathol Exp Neurol* 1999;**58**:795–802. doi:10.1097/00005072-199908000-00002.

[24] Baumann P, Cremers N, Kroese F, Orend G, Chiquet-Ehrismann R, Uede T, Yagita H, Sleeman JP. CD24 expression causes the acquisition of multiple cellular properties associated with tumor growth and metastasis. *Cancer Res* 2005;**65**:10783–93. doi:10.1158/0008-5472.CAN-05-0619.

[25] Kristiansen G, Winzer K-J, Mayordomo E, Bellach J, Schlüns K, Denkert C, Dahl E, Pilarsky C, Altevogt P, Guski H, Dietel M. CD24 expression is a new prognostic marker in breast cancer. *Clin Cancer Res* 2003;**9**:4906–13.

[26] Deng J, Gao G, Wang L, Wang T, Yu J, Zhao Z. CD24 expression as a marker for predicting clinical outcome in human gliomas. *J Biomed Biotechnol* 2012;**2012**:517172. doi:10.1155/2012/517172.

[27] Clarke MF. Self-renewal and solid-tumor stem cells. *Biol Blood Marrow Transplant* 2005;**11**:14–16. doi:10.1016/j.bbmt.2004.11.011.

[28] Batlle E, Clevers H. Cancer stem cells revisited. *Nat Med* 2017;**23**:1124–34. doi:10.1038/nm.4409.

[29] Chen J, Li Y, Yu T-S, McKay RM, Burns DK, Kernie SG, Parada LF. A restricted cell population propagates glioblastoma growth after chemotherapy. *Nature* 2012;**488**:522–6. doi:10.1038/nature11287.

[30] Bao S, Wu Q, McLendon RE, Hao Y, Shi Q, Hjelmeland AB, Dewhirst MW, Bigner DD, Rich JN. Glioma stem cells promote radioresistance by preferential activation of the DNA damage response. *Nature* 2006;**444**:756–60. doi:10.1038/nature05236.

[31] Liau BB, Sievers C, Donohue LK, Gillespie SM, Flavahan WA, Miller TE, Venteicher AS, Hebert CH, Carey CD, Rodig SJ, Shareef SJ, Najm FJ, van Galen P, Wakimoto H, Cahill DP, Rich JN, Aster JC, Suvà ML, Patel AP, Bernstein BE. Adaptive chromatin remodeling drives glioblastoma stem cell plasticity and drug tolerance. *Cell Stem Cell* 2017;**20** 233-246.e7. doi:10.1016/j.stem.2016.11.003.

[32] Li C, Heidt DG, Dalerba P, Burant CF, Zhang L, Adsay V, Wicha M, Clarke MF, Simeone DM. Identification of pancreatic cancer stem cells. *Cancer Res* 2007;**67**:1030–7. doi:10.1158/0008-5472.CAN-06-2030.

[33] Vermeulen L, Todaro M, de Sousa Mello F, Sprick MR, Kemper K, Perez Alea M, Richel DJ, Stassi G, Medema JP. Single-cell cloning of colon cancer stem cells reveals a multi-lineage differentiation capacity. *Proc Natl Acad Sci USA.* 2008;**105**:13427–32. doi:10.1073/pnas.0805706105.

[34] Lee TKW, Castilho A, Cheung VCH, Tang KH, Ma S, Ng IOL. CD24(+) liver tumor-initiating cells drive self-renewal and tumor initiation through STAT3-mediated NANOG regulation. *Cell Stem Cell* 2011;**9**:50–63. doi:10.1016/j.stem.2011.06.005.

[35] Liu AY, Cai Y, Mao Y, Lin Y, Zheng H, Wu T, Huang Y, Fang X, Lin S, Feng Q, Huang Z, Yang T, Luo Q, Ouyang G. Twist2 promotes self-renewal of liver cancer stem-like cells by regulating CD24. *Carcinogenesis* 2014;**35**:537–45. doi:10.1093/carcin/bgt364.

[36] Yang C-H, Wang H-L, Lin Y-S, Kumar KPS, Lin H-C, Chang C-J, Lu C-C, Huang T-T, Martel J, Ojcius DM, Chang Y-S, Young JD, Lai H-C. Identification of CD24 as a cancer stem cell marker in human nasopharyngeal carcinoma. *PLoS One* 2014;**9**:e99412. doi:10.1371/journal.pone.0099412.

[37] Hansford LM, McKee AE, Zhang L, George RE, Gerstle JT, Thorner PS, Smith KM, Look AT, Yeger H, Miller FD, Irwin MS, Thiele CJ, Kaplan DR. Neuroblastoma cells isolated from bone marrow metastases contain a naturally enriched tumor-initiating cell. *Cancer Res* 2007;**67**:11234–43. doi:10.1158/0008-5472.CAN-07-0718.

[38] Rohle D, Popovici-Muller J, Palaskas N, Turcan S, Grommes C, Campos C, Tsoi J, Clark O, Oldrini B, Komisopoulou E, Kunii K, Pedraza A, Schalm S, Silverman L, Miller A, Wang F, Yang H, Chen Y, Kernytsky A, Rosenblum MK, Mellinghoff IK. An inhibitor of mutant IDH1 delays growth and promotes differentiation of glioma cells. *Science* 2013;**340**:626–30. doi:10.1126/science.1236062.

[39] Turcan S, Fabius AWM, Borodovsky A, Pedraza A, Brennan C, Huse J, Viale A, Riggins GJ, Chan TA. Efficient induction of differentiation and growth inhibition in IDH1 mutant glioma cells by the DNMT Inhibitor Decitabine. *Oncotarget* 2013;**4**:1729–36. doi:10.18632/oncotarget.1412.

[40] Park J-W, Sahm F, Steffl B, Arrillaga-Romany I, Cahill D, Monje M, Herold-Mende C, Wick W, Turcan Ş. TERT and DNMT1 expression predict sensitivity to decitabine in gliomas. *Neuro Oncol* 2021;**23**:76–87. doi:10.1093/neuonc/noaa207.

[41] Weber E, Lehmann HP, Beck-Sickinger AG, Wawrzynczak EJ, Waibel R, Folkers G, Stahel RA. Antibodies to the protein core of the small cell lung cancer workshop antigen cluster-w4 and to the leucocyte workshop antigen CD24 recognize the same short protein sequence leucine-alanine-proline. *Clin Exp Immunol* 1993;**93**:279–85. doi:10.1111/j.1365-2249.1993.tb07980.x.

[42] Kristiansen G, Machado E, Bretz N, Rupp C, Winzer K-J, König A-K, Moldenhauer G, Marmé F, Costa J, Altevogt P. Molecular and clinical dissection

of CD24 antibody specificity by a comprehensive comparative analysis. *Lab Invest* 2010;**90**:1102–16. doi:10.1038/labinvest.2010.70.

[43] Yu G, Wang L-G, Han Y, He Q-Y. clusterProfiler: an R package for comparing biological themes among gene clusters. *OMICS* 2012;**16**:284–7. doi:10.1089/omi.2011.0118.

[44] Wu T, Hu E, Xu S, Chen M, Guo P, Dai Z, Feng T, Zhou L, Tang W, Zhan L, Fu X, Liu S, Bo X, Yu G. clusterProfiler 4.0: A universal enrichment tool for interpreting omics data. *Innovation (N Y)* 2021;**2**:100141. doi:10.1016/j.xinn.2021.100141.

[45] Yu G, He Q-Y. ReactomePA: an R/Bioconductor package for reactome pathway analysis and visualization. *Mol Biosyst* 2016;**12**:477–9. doi:10.1039/c5mb00663e.

[46] Dobin A, Davis CA, Schlesinger F, Drenkow J, Zaleski C, Jha S, Batut P, Chaisson M, Gingeras TR. STAR: ultrafast universal RNA-seq aligner. *Bioinformatics* 2013;**29**:15–21. doi:10.1093/bioinformatics/bts635.

[47] Dobin A, Gingeras TR. Mapping RNA-seq Reads with STAR. *Curr. Protoc. Bioinformatics.* 2015;**51** 11.14.1-11.14.19. doi:10.1002/0471250953.bi1114s51.

[48] Liao Y, Smyth GK, Shi W. featureCounts: an efficient general purpose program for assigning sequence reads to genomic features. *Bioinformatics* 2014;**30**:923–30. doi:10.1093/bioinformatics/btt656.

[49] Love MI, Huber W, Anders S. Moderated estimation of fold change and dispersion for RNA-seq data with DESeq2. *Genome Biol* 2014;**15** 550–550. doi:10.1186/s13059-014-0550-8.

[50] Subramanian A, Tamayo P, Mootha VK, Mukherjee S, Ebert BL, Gillette MA, Paulovich A, Pomeroy SL, Golub TR, Lander ES, Mesirov JP. Gene set enrichment analysis: a knowledge-based approach for interpreting genome-wide expression profiles. *Proc Natl Acad Sci USA.* 2005;**102**:15545–50. doi:10.1073/pnas.0506580102.

[51] Mootha VK, Lindgren CM, Eriksson K-F, Subramanian A, Sihag S, Lehar J, Puigserver P, Carlsson E, Ridderstråle M, Laurila E, Houstis N, Daly MJ, Patterson N, Mesirov JP, Golub TR, Tamayo P, Spiegelman B, Lander ES, Hirschhorn JN, Altshuler D, Groop LC. PGC-1alpha-responsive genes involved in oxidative phosphorylation are coordinately downregulated in human diabetes. *Nat Genet* 2003;**34**:267–73. doi:10.1038/ng1180.

[52] Liberzon A, Subramanian A, Pinchback R, Thorvaldsdóttir H, Tamayo P, Mesirov JP. Molecular signatures database (MSigDB) 3.0. *Bioinformatics* 2011;**27**:1739–40. doi:10.1093/bioinformatics/btr260.

[53] Liberzon A, Birger C, Thorvaldsdóttir H, Ghandi M, Mesirov JP, Tamayo P. The Molecular Signatures Database (MSigDB) hallmark gene set collection. *Cell Syst* 2015;**1**:417–25. doi:10.1016/j.cels.2015.12.004.

[54] Wiederschain D, Wee S, Chen L, Loo A, Yang G, Huang A, Chen Y, Caponigro G, Yao Y-M, Lengauer C, Sellers WR, Benson JD. Single-vector inducible lentiviral RNAi system for oncology target validation. *Cell Cycle* 2009;**8**:498–504. doi:10.4161/cc.8.3.7701.

[55] Turkekul M, Barlas A, Yarilin D, Fujisawa S, Fan N, Brendel M, Manova-Todorova K. Automated Double In Situ Detection of Mouse Lgr5 mRNA and Lysozyme Protein in Examining the Neighboring Cell Types of the Mouse Intestinal Crypt. *Methods Mol Biol* 2017;**1554**:263–72. doi:10.1007/978-1-4939-6759-9_19.

[56] Schindelin J, Arganda-Carreras I, Frise E, Kaynig V, Longair M, Pietzsch T, Preibisch S, Rueden C, Saalfeld S, Schmid B, Tinevez J-Y, White DJ, Hartenstein V, Eliceiri K, Tomancak P, Cardona A. Fiji: an open-source platform for biological-image analysis. *Nat. Methods.* 2012;**9**:676–82. doi:10.1038/nmeth.2019.

[57] Counter CM, Hahn WC, Wei W, Caddle SD, Beijersbergen RL, Lansdorp PM, Sedivy JM, Weinberg RA. Dissociation among in vitro telomerase activity, telomere maintenance, and cellular immortalization. *Proc Natl Acad Sci USA.* 1998;**95**:14723–8. doi:10.1073/pnas.95.25.14723.

[58] Network Cancer Genome Atlas Research, Brat DJ, Verhaak RGW, Aldape KD, Yung WKA, Salama SR, Cooper LAD, Rheinbay E, Miller CR, Vitucci M, Morozova O, Robertson AG, Noushmehr H, Laird PW, Cherniack AD, Akbani R, Huse JT, Ciriello G, Poisson LM, Barnholtz-Sloan JS, et al. Comprehensive, Integrative Genomic Analysis of Diffuse Lower-Grade Gliomas. *N Engl J Med* 2015;**372**:2481–98. doi:10.1056/NEJMoa1402121.

[59] Vescovi AL, Snyder EY. Establishment and properties of neural stem cell clones: plasticity in vitro and in vivo. *Brain Pathol* 1999;**9**:569–98. doi:10.1111/j.1750-3639.1999.tb00542.x.

[60] Weiss S, Dunne C, Hewson J, Wohl C, Wheatley M, Peterson AC, Reynolds BA. Multipotent CNS stem cells are present in the adult mammalian spinal cord and ventricular neuroaxis. *J Neurosci* 1996;**16**:7599–609. doi:10.1523/JNEUROSCI.16-23-07599.1996.

[61] Lee J, Kotliarova S, Kotliarov Y, Li A, Su Q, Donin NM, Pastorino S, Purow BW, Christopher N, Zhang W, Park JK, Fine HA. Tumor stem cells derived from glioblastomas cultured in bFGF and EGF more closely mirror the phenotype and genotype of primary tumors than do serum-cultured cell lines. *Cancer Cell* 2006;**9**:391–403. doi:10.1016/j.ccr.2006.03.030.

[62] Lathia JD, Mack SC, Mulkearns-Hubert EE, Valentim CLL, Rich JN. Cancer stem cells in glioblastoma. *Genes Dev* 2015;**29**:1203–17. doi:10.1101/gad.261982.115.

[63] Singh SK, Clarke ID, Terasaki M, Bonn VE, Hawkins C, Squire J, Dirks PB. Identification of a cancer stem cell in human brain tumors. *Cancer Res* 2003;**63**:5821–8.

[64] Singh SK, Hawkins C, Clarke ID, Squire JA, Bayani J, Hide T, Henkelman RM, Cusimano MD, Dirks PB. Identification of human brain tumour initiating cells. *Nature* 2004;**432**:396–401. doi:10.1038/nature03128.

[65] Galli R, Binda E, Orfanelli U, Cipelletti B, Gritti A, De Vitis S, Fiocco R, Foroni C, Dimeco F, Vescovi A. Isolation and characterization of tumorigenic, stem-like neural precursors from human glioblastoma. *Cancer Res* 2004;**64**:7011–21. doi:10.1158/0008-5472.CAN-04-1364.

[66] Thomas S, Harding MA, Smith SC, Overdevest JB, Nitz MD, Frierson HF, Tomlins SA, Kristiansen G, Theodorescu D. CD24 is an effector of HIF-1-driven primary tumor growth and metastasis. *Cancer Res* 2012;**72**:5600–12. doi:10.1158/0008-5472.CAN-11-3666.

[67] Doetsch F, Caillé I, Lim DA, García-Verdugo JM, Alvarez-Buylla A. Subventricular zone astrocytes are neural stem cells in the adult mammalian brain. *Cell* 1999;**97**:703–16. doi:10.1016/s0092-8674(00)80783-7.

[68] Doetsch F, Petreanu L, Caille I, Garcia-Verdugo JM, Alvarez-Buylla A. EGF converts transit-amplifying neurogenic precursors in the adult brain into multipotent stem cells. *Neuron* 2002;**36**:1021–34. doi:10.1016/s0896-6273(02)01133-9.

[69] Dulken BW, Leeman DS, Boutet SC, Hebestreit K, Brunet A. Single-Cell Transcriptomic Analysis Defines Heterogeneity and Transcriptional Dynamics in the Adult Neural Stem Cell Lineage. *Cell Rep* 2017;**18**:777–90. doi:10.1016/j.celrep.2016.12.060.

[70] Raponi E, Agenes F, Delphin C, Assard N, Baudier J, Legraverend C, Deloulme J-C. S100B expression defines a state in which GFAP-expressing cells lose their neural stem cell potential and acquire a more mature developmental stage. *Glia* 2007;**55**:165–77. doi:10.1002/glia.20445.

[71] Zarn JA, Zimmermann SM, Pass MK, Waibel R, Stahel RA. Association of CD24 with the kinase c-fgr in a small cell lung cancer cell line and with the kinase lyn in an erythroleukemia cell line. *Biochem Biophys Res Commun* 1996;**225**:384–91. doi:10.1006/bbrc.1996.1184.

[72] Baumann P, Thiele W, Cremers N, Muppala S, Krachulec J, Diefenbacher M, Kassel O, Mudduluru G, Allgayer H, Frame M, Sleeman JP. CD24 interacts with and promotes the activity of c-src within lipid rafts in breast cancer cells, thereby increasing integrin-dependent adhesion. *Cell Mol Life Sci* 2012;**69**:435–48. doi:10.1007/s00018-011-0756-9.

[73] Bretz NP, Salnikov AV, Perne C, Keller S, Wang X, Mierke CT, Fogel M, Erbe-Hofmann N, Schlange T, Moldenhauer G, Altevogt P. CD24 controls Src/STAT3 activity in human tumors. *Cell. Mol. Life Sci* 2012;**69**:3863–79. doi:10.1007/s00018-012-1055-9.

[74] Su N, Peng L, Xia B, Zhao Y, Xu A, Wang J, Wang X, Jiang B. Lyn is involved in CD24-induced ERK1/2 activation in colorectal cancer. *Mol. Cancer.* 2012;**11**:43. doi:10.1186/1476-4598-11-43.

[75] Aigner S, Sthoeger ZM, Fogel M, Weber E, Zarn J, Ruppert M, Zeller Y, Vestweber D, Stahel R, Sammar M, Altevogt P. CD24, a mucin-type glycoprotein, is a ligand for P-selectin on human tumor cells. *Blood* 1997;**89**:3385–95. doi:10.1182/blood.V89.9.3385.

[76] Myung JH, Gajjar KA, Pearson RM, Launiere CA, Eddington DT, Hong S. Direct measurements on CD24-mediated rolling of human breast cancer MCF-7 cells on E-selectin. *Anal Chem* 2011;**83**:1078–83. doi:10.1021/ac102901e.

[77] Barkal AA, Brewer RE, Markovic M, Kowarsky M, Barkal SA, Zaro BW, Krishnan V, Hatakeyama J, Dorigo O, Barkal LJ, Weissman IL. CD24 signalling through macrophage Siglec-10 is a target for cancer immunotherapy. *Nature* 2019;**572**:392–6. doi:10.1038/s41586-019-1456-0.